$CuWO_4$ decorated ZnO corn kernels-like nanostructure for enhanced photocatalytic activity

S. Wannapop *, T. Phancharoen, K. Benphad, A. Somdee
Faculty of Science, Energy, and Environment, King Mongkut's University of Technology North Bangkok, Rayong Campus, Rayong 21120, Thailand

The reflux method was successfully employed to synthesize a $CuWO_4$-decorated zine oxide (ZnO) corn kernel-like nanostructure. X-ray diffraction analysis revealed that the $CuWO_4$ and ZnO corn kernel-like nanostructures exhibit anorthic and hexagonal structures, respectively. The composite structure of $CuWO_4$-decorated ZnO was composed of two phases: the hexagonal ZnO and the anorthic $CuWO_4$. The photodegradation of rhodamine B was tested using $CuWO_4$, ZnO, and various $CuWO_4$-decorated ZnO photocatalysts under solar radiation for 140 min. Among the photocatalysts tested, 10% $CuWO_4$-decorated ZnO exhibited the highest photocatalytic activity. Additionally, this material demonstrated high stability and reusability over three consecutive photocatalytic tests.

(Received November 23, 2024; Accepted February 21, 2025)

Keywords: $CuWO_4$, Photocatalysis, SEM, TEM, ZnO

1. Introduction

Water pollution refers to a pressing global issue that adversely affects aquatic ecosystems, wildlife, and human health, necessitating immediate attention. Pollution can originate from various sources, such as agricultural activities, households, and industry. Some of the substances in water pollution can be difficult to remove. The photocatalytic process offers a promising solution to this problem due to its eco-friendly nature [1], chemical and thermal stability [2], broad applicability to different pollutants [3], and energy efficiency through the use of solar power [4].

Zinc oxide (ZnO) is a compelling photocatalyst for organic dye removal due to its cost-effectiveness, easy-to-control surface and morphology, high electron mobility, and environmental friendliness [5]. Despite its potential, ZnO faces limitations such as visible light absorption [6], rapid recombination of charge carriers [7], and photo corrosion [8]. Researchers are exploring strategies to overcome these limitations, including doping ZnO with different metals or non-metals and coupling it with other semiconductors to create heterostructures [9–14].

Transition metal tungstates (MWO_4, where M is a metal) are a type of metal oxide that has recently gained attention for their promising photocatalytic performance. Because of their strong adsorption ability, these materials possess unique properties, such as narrow band gaps and excellent catalytic activity [15–16], making them highly effective for photocatalytic applications. Copper tungstate ($CuWO_4$) is an excellent choice for various photocatalytic processes [17–18] due to its unique properties, including appropriate frequency bands for absorption of visible light, superior catalytic performance, and exceptional chemical stability. [19–22]. Combining $CuWO_4$ and ZnO for photocatalytic applications shows an exciting potential for improving photocatalytic efficiency. By decorating ZnO with $CuWO_4$, several synergistic effects can be achieved, leading to enhanced performance in various photocatalytic processes.

In this study, $CuWO_4$ was successfully prepared using a hydrothermal method, while a reflux method was used to synthesize $CuWO_4$-decorated ZnO. The morphology, optical properties, and surface areas of the catalysts were analyzed. The catalyst products of $CuWO_4$, ZnO, and

* Corresponding author: surangkana.w@sciee.kmutnb.ac.th
https://doi.org/10.15251/DJNB.2025.201.201

$CuWO_4$-decorated ZnO were investigated through photocatalytic activity using rhodamine B (RhB) solutions under solar radiation.

2. Experimental

$CuWO_4$ was synthesized hydrothermally. 3 mmol of $Cu(NO_3)_2 \cdot 3H_2O$ was dissolved in 30 mL of deionized (DI) water, while 3 mmol of $Na_2W_{O4} \cdot 5H_2O$ was dissolved in another 30 mL of DI water. The two solutions were then mixed vigorously for 30 minutes. The mixture was then transferred to a 100 mL Teflon line of a hydrothermal reaction and placed in an autoclave at 180 °C for 24 h. The final products were rinsed with DI water and ethanol and dried at 80 °C for 24 hours. The sample was labeled as CWO.

A ZnO corn kernel-like nanostructure was synthesized using the reflux method. Initially, 5 mmol of $Zn(CH_3COOH)_2$ was solubilized in 50 mL DI water, and 0.01 mol of NaOH was solubilized in 50 mL DI water. These solutions were mixed and subjected to the reflux method at 100 °C for 1 h. The resulting product was cleaned with DI water and ethanol before being dried at 80 °C for 24 h.

$CuWO_4$-decorated ZnO was synthesized using a reflux method similar to that for the pure ZnO corn kernel-like nanostructure. In this process, $CuWO_4$ powder was added to the synthesis mixture in concentrations of 10 and 20 wt% relative to $Zn(CH_3COOH)_2$. The samples were designated 10CWO/ZnO and 20CWO/ZnO, respectively.

The products were characterized using various techniques, namely X-ray diffraction (XRD) with a Bruker AXS D8 eco, transmission electron microscopy (TEM) with a JEOL instrument (JEOL JEM-2010), scanning electron microscopy (SEM) using a JEOL JSM 6335F, the Brunauer-Emmett-Teller (BET) method with a Quantachrome Instruments Autosorb-iQ-MP-MP, and X-ray photoelectron spectroscopy (XPS) utilizing an Axis Ultra DLD. Photoluminescent spectra (PL, JASCO, FP-8500) were obtained by exciting the sample with a laser at a wavelength of 325 nm, and the emitted light was collected and analyzed.

The photocatalytic activity of the products was investigated through the photodegradation of RhB solutions using a xenon lamp with a constant light intensity. For this evaluation, 0.2 g of the catalyst was dispersed in 200 mL of a 1×10^{-5} M RhB aqueous solution. The mixed specimen was kept in the dark for 30 minutes while being stirred magnetically. A 5 mL sample of the solution was sampled and centrifuged every 10 minutes during photocatalytic testing. The residual of RhB concentration was measured at the peak absorption wavelength of 553 nm using UV-visible spectrophotometry (Shimadzu UV-2600).

3. Results and discussion

The XRD patterns of ZnO, $CuWO_4$, and $CuWO_4$-decorated ZnO at 10 and 20 wt% $CuWO_4$ concentrations were shown in Fig. 1a. The diffraction peaks indicate that the $CuWO_4$-decorated ZnO samples consist of two phases: hexagonal ZnO (JCPDS no. 36-1451) and anorthic $CuWO_4$ (JCPDS no. 70-1732) [22–23]. The XPS survey scans for the pure ZnO, $CuWO_4$, and $CuWO_4$-decorated ZnO samples are displayed in Fig. 1b, while the XPS peaks for Zn, O, Cu, and W are shown in Figs. 2a–d, respectively. In Fig. 2a, the peaks for zinc are assigned to the spin-orbit splitting of the zinc $2p_{3/2}$ and $2p_{1/2}$ energy levels. The high-resolution O 1s peak (Fig. 2b) exhibited multiple overlapping components. This peak was fitted with a Gaussian function and resolved with binding energies of 529.25, 530.23, 531.33, and 532.33 eV, representing Zn–O, oxygen species in $CuWO_4$, Zn–OH, and oxygen species in $CuWO_4$, respectively [18]. Fig. 2c shows that the spin-orbit peaks for copper are Cu 2p3/2 and Cu 2p1/2, which appear at 932.98 eV and 952.47 eV, respectively. The tungsten peaks at 34.65 eV and 36.81 eV in Fig. 2d correspond to the spin-orbit-split W 4f7/2 and W 4f5/2, respectively.

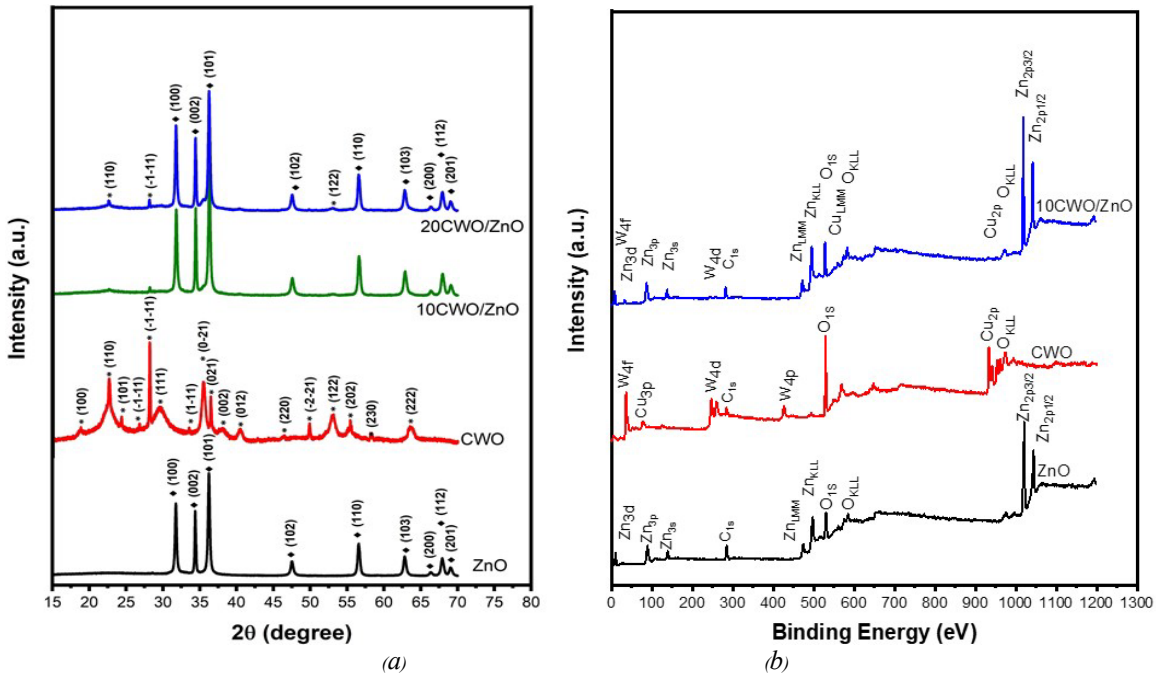

(a) *(b)*

Fig. 1. (a) XRD patterns of ZnO, CWO, 10CWO/ZnO, and 20CWO/ZnO; (b) XPS survey scan of ZnO, CWO, and 10CWO/ZnO.

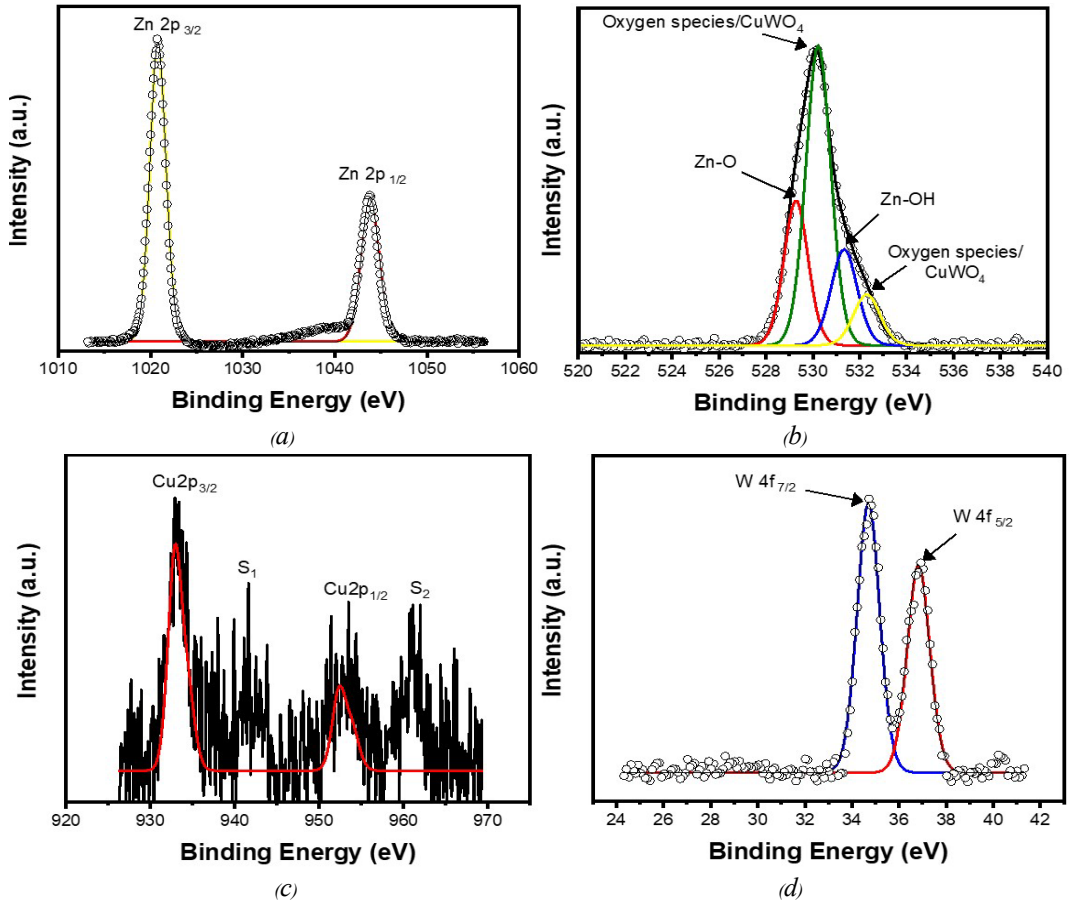

(a) *(b)* *(c)* *(d)*

Fig. 2. High-resolution XPS spectroscopy of 10CWO/ZnO: (a) Zn 2p XPS spectra of 10CWO/ZnO, (b) O 1s spectra of 10CWO/ZnO, (c) Cu 2p spectra of 10CWO/ZnO, and (d) W 4f spectra of 10CWO/ZnO.

Fig. 3 shows an SEM image of pure ZnO, $CuWO_4$, and $CuWO_4$-decorated ZnO. Pure ZnO exhibits a corn kernel-like nanostructure, while $CuWO_4$ appears as nanoparticles. Upon decorating ZnO with $CuWO_4$, the surface roughness of ZnO increases proportionally with the concentration of $CuWO_4$. Fig. 3f–i demonstrate that energy-dispersive X-ray spectroscopy (EDX) maps indicate the presence of $CuWO_4$ in 10CWO/ZnO. Additionally, the EDX maps confirm that $CuWO_4$ is situated on the surface of ZnO, aligning with the results from the TEM image.

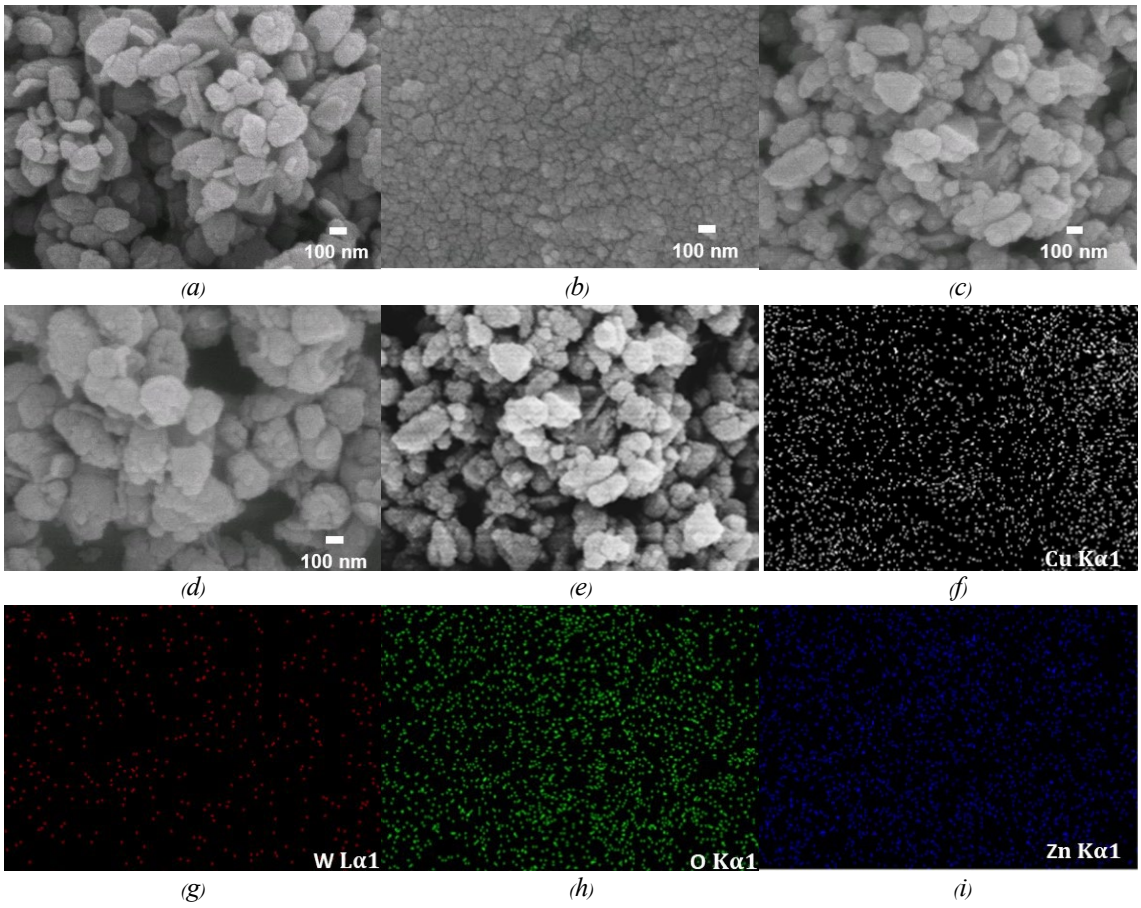

Fig. 3. SEM images of (a) ZnO, (b) CWO, (c) 10CWO/ZnO, (d) 20CWO/ZnO, (e) backscattered electron image of 10CWO/ZnO, and (f–i) EDX maps of 10CWO/ZnO.

Fig.4a demonstrates a TEM image of $CuWO_4$ nanoparticles. The average $CuWO_4$ particle size, as illustrated in Fig. 4c, was about 16.63 nm. The high-resolution transmission electron microscopy HRTEM) image of CWO demonstrates that the lattice fringes correspond to the (–110) planes of anorthic $CuWO_4$. Fig. 4d shows the corn kernel-like nanostructure of ZnO, while HRTEM (Fig. 4e) indicates that the lattice fringes correspond to (101) planes from hexagonal ZnO. The average ZnO particle size, as illustrated in Fig. 4f, was approximately 181.87 nm. Upon decoration with $CuWO_4$, the surface roughness of ZnO (and size of ZnO) increases proportionally with the concentration of $CuWO_4$, aligning with SEM analysis. The HRTEM image of 10CWO/ZnO and 20CWO/ZnO shows that $CuWO_4$ can decorate the surface of ZnO, with the lattice fringes corresponding to (120) and (–110) planes from anorthic $CuWO_4$.

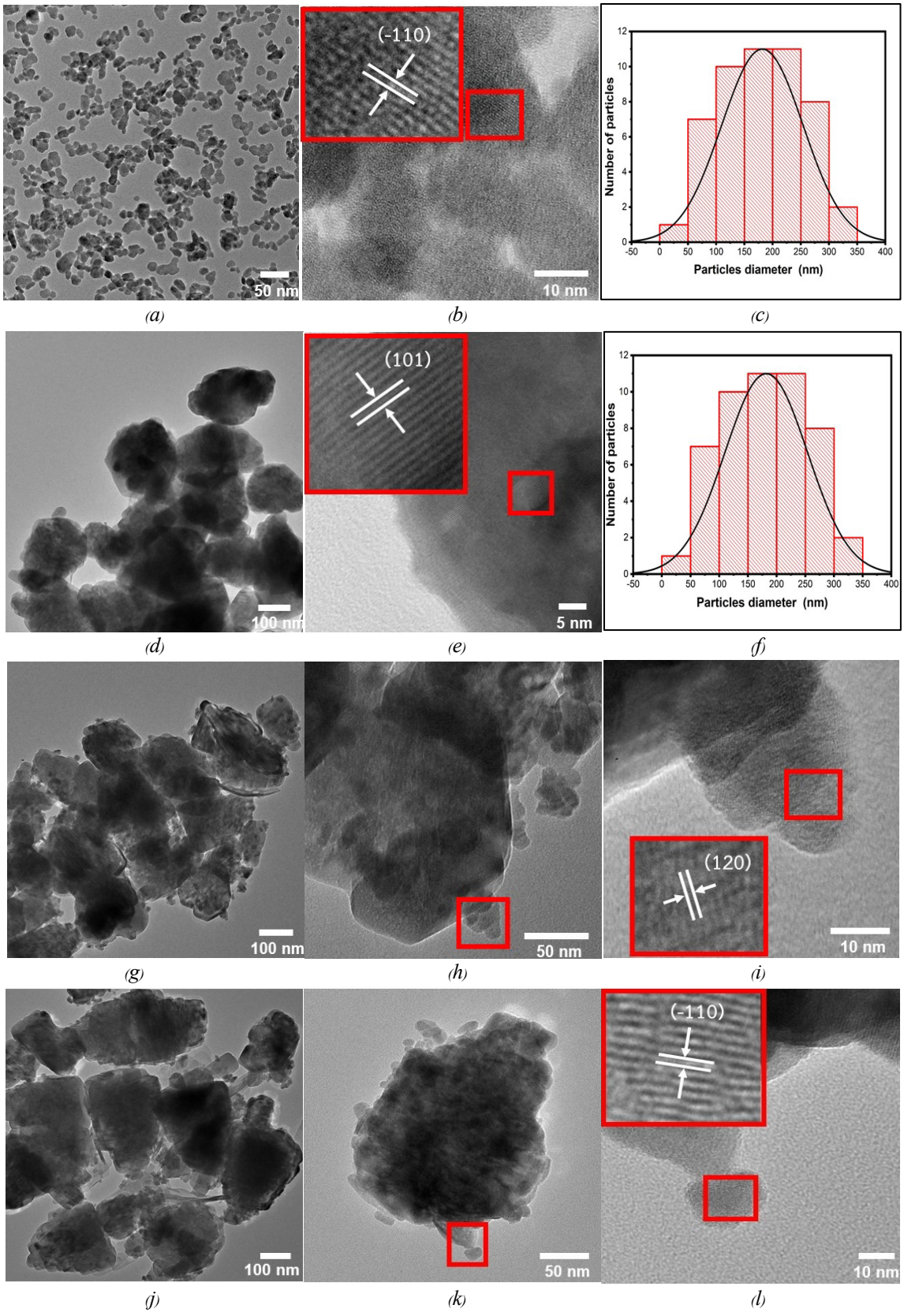

Fig. 4. TEM images, HRTEM images, and particle diameter histograms: (a–c) CWO, (d–f) ZnO, (g–i) 10CWO/ZnO, and (j–l) 20CWO/ZnO.

The optical absorption properties of ZnO, $CuWO_4$, and $CuWO_4$-decorated ZnO were effectively characterized using UV-visible spectroscopy, as depicted in Fig. 5a. In this analysis, the $CuWO_4$-decorated ZnO products show excellent absorption compared to pure ZnO. The energy band gap of ZnO, $CuWO_4$, and ZnO modified by $CuWO_4$ was determined using the Kubelka-Munk function.

$$(\alpha hv)^2 = A(hv - Eg) \quad (1)$$

where α, hv, A, and Eg represent the material absorption coefficient, light energy, a constant, and band gap energy, respectively. [24]. Fig. 5b illustrates the band gap energies of ZnO, CWO, 10CWO/ZnO, and 20CWO/ZnO, which were determined to be 3.19 eV, 2.54 eV, 3.15 eV, and 3.17 eV, respectively. [24–25]. This indicates that, as $CuWO_4$ had a smaller band gap energy than pure ZnO, it decreased the band gap energy of $CuWO_4$-decorated ZnO. The photocatalytic activities of ZnO and $CuWO_4$-decorated ZnO catalysts were evaluated by degrading RhB molecules under simulated solar radiation.

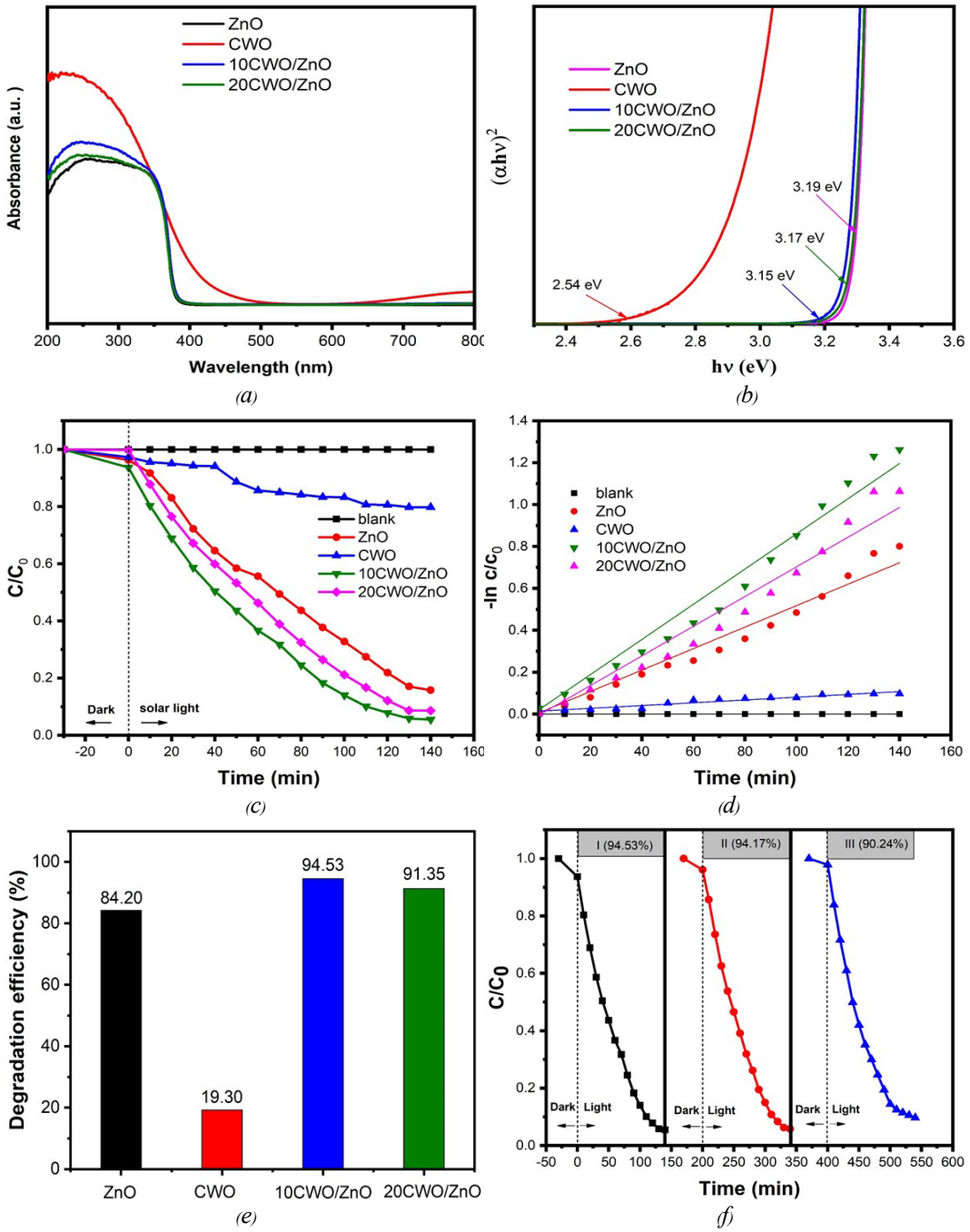

Fig. 5. (a) UV-Visibility spectra; (b) band gap energies; (c) Curves of C/C_0 versus time for the photodegradation of RhB; (d) pseudo-first-order plot for photodegradation; (e) degradation efficiency using RhB for ZnO, CWO, 10CWO/ZnO, and 20 CWO/ZnO; and (f) recycling of 10CWO/ZnO under simulated solar light.

Figs. 5c–e depicts the decolorization efficiency of the RhB solution, used as a model dye, under blank conditions (catalyst-free), as well as with ZnO, $CuWO_4$, and $CuWO_4$-decorated ZnO photocatalysts for 140 minutes. The RhB dye absorption ability of ZnO, CWO, 10CWO/ZnO, and 20CWO/ZnO before solar simulator irradiation was 3.69%, 2.69%, 6.27%, and 0.165%, respectively. 10CWO/ZnO demonstrated a better ability to absorb RhB dye than pure ZnO and 20CWO/ZnO, consistent with the BET results. However, CWO had the highest surface area compared to the other samples but absorbed less RhB than 10CWO/ZnO, likely due to pores on the surface. The efficiency values of RhB dye treatment for ZnO, CWO, 10CWO/ZnO, and 20CWO/ZnO were 84.20%, 19.30%, 94.53%, and 91.35%, respectively. For 140 min, 10CWO/ZnO

showed the highest decolorization efficiency of 94.53%. The stability of the reused 10CWO/ZnO composite was evaluated through repeated degradation of RhB over three cycles, as illustrated in Fig. 5f. By the end of the third cycle, the photodegradation efficiency for RhB using 10CWO/ZnO had decreased to 90.24%. This result demonstrates that 10CWO/ZnO is highly stable and can be reused effectively under simulated solar light conditions.

Fig. 6a displays the photoluminescence spectra of ZnO, $CuWO_4$, and $CuWO_4$-decorated ZnO. The unmodified ZnO exhibited the highest peak intensity, indicating a strong tendency for electrons and holes to recombine on its surface. The decoration of $CuWO_4$ on the surface of ZnO caused to a significant decrease in the peak intensity of ZnO. This suggests that $CuWO_4$ can separate the electron-hole pairs created by light, improving photocatalytic performance [26]. The surface areas of ZnO, $CuWO_4$, 10CWO/ZnO, and 20CWO/ZnO were also analyzed using Brunauer-Emmet-Teller analysis. The surface areas of ZnO, $CuWO_4$, 10CWO/ZnO, and 20CWO/ZnO were 16.88, 50.58, 17.92, and 13.26 m^2/g, respectively. $CuWO_4$ had the largest surface area, followed by 10CWO/ZnO, ZnO, and 20CWO/ZnO. The results imply that modifying the surface of ZnO with $CuWO_4$ can decrease electron recombination, consistent with the lower peak concentration observed in the PL spectra. The modified ZnO demonstrates greater photocatalytic efficiency than $CuWO_4$ and pure ZnO. $CuWO_4$ has a smaller band gap than ZnO and $CuWO_4$-decorated ZnO, as it increases electron recombination. This makes it less effective in treating dyes than ZnO and modified ZnO, even though $CuWO_4$ has a higher relative surface area. This explains why the efficiency degradation of $CuWO_4$-decorated ZnO is better than that of $CuWO_4$ and pure ZnO. However, regarding RhB dye treatment, the improved performance of 10CWO/ZnO compared with 20CWO/ZnO can be attributed to its better light absorption capacity and larger surface area. These factors significantly enhance the separation of electron-hole pairs and increase the availability of active sites for catalytic reactions, resulting in superior photocatalytic activity.

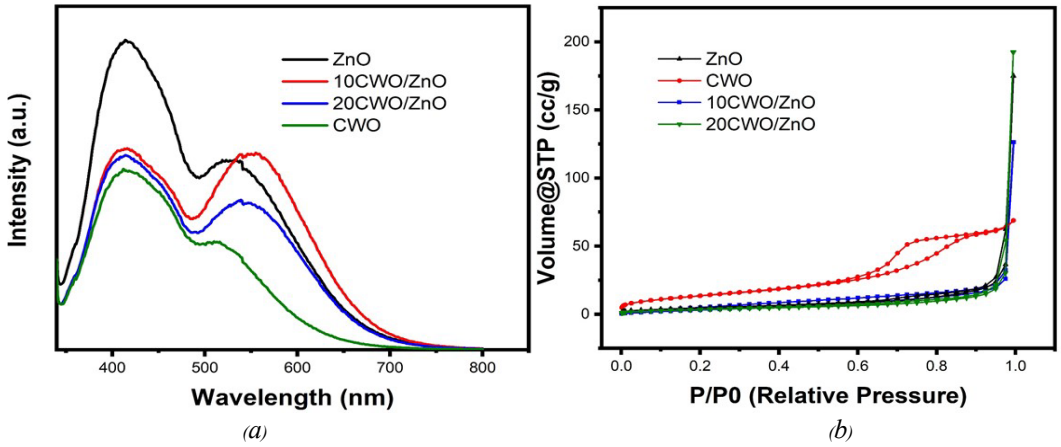

Fig. 6. (a) Photoluminescent spectra; and (b) Brunauer-Emmet-Teller analysis of ZnO, CWO, 10CWO/ZnO, and 20CWO/ZnO.

The proposed $CuWO_4$-decorated ZnO photocatalytic mechanism is shown in Fig. 7. Upon the light absorption, the electrons in the conduction band (CB) of ZnO are excited, causing them to transition from the valence band (VB) to the CB, thereby leaving behind holes in the VB. These holes (h^+) participate in a redox reaction with absorbed dye molecules. The holes in the VB reduced an electron of the water molecule or hydroxide ions (OH^-) to produce hydroxide radicals ($^{\cdot}H$). Meanwhile, the photo-generated electrons (e^-) are migrated to the surface of $CuWO_4$ and participate in reduction reactions. Thus, the photo-generated electrons and holes act as reactive species. Owing to its distinctive electronic structure, $CuWO_4$ facilitates the generation and recombination of charge carriers [26].

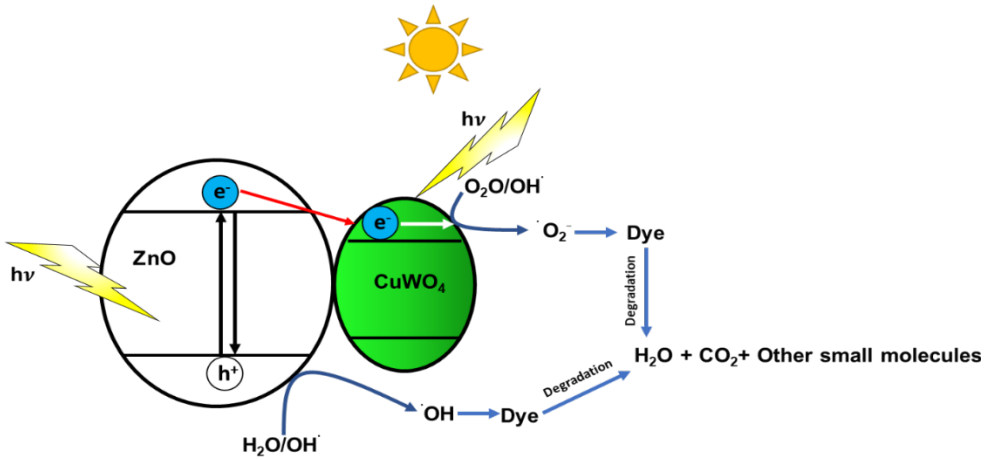

Fig. 7. Proposed $CuWO_4$-decorated ZnO composites photocatalytic mechanism for the RhB degradation under simulated sunlight illumination.

4. Conclusions

$CuWO_4$-decorated ZnO was successfully synthesized using the reflux method. Then, its photocatalytic activities were evaluated through photodegradation experiments. The 10CWO/ZnO photocatalyst exhibited superior performance in RhB degradation compared with the other samples. This material demonstrated excellent stability and reusability, highlighting its potential for real-world wastewater treatment applications. The findings indicate that the $CuWO_4$-decorated ZnO photocatalyst enhanced the ZnO-based material to become a strong photocatalyst material, and it is a good candidate for wastewater treatment.

Acknowledgments

This research was funded by the National Science, Research and Innovation Fund (NSRF), and King Mongkut's University of Technology North Bangkok with contract no. KMUTNB-FF-65-51.

References

[1] P. Ponnarasi, G. Mahalakshmi, Chem. Phys. 8, 100632(2024); https://doi.org/10.1016/j.chphi.2024.100632

[2] Y. Liu, M. Shan, L. Du, W. Sun, D. Wu, Q. Bi, H. Wang, Y. Liu, Appl. Surf. Sci. 623, 157006(2023); https://doi.org/10.1016/j.apsusc.2023.157006

[3] S. Rawat, J. Sing, J. Environ. Manage. 318, 115518(2022); https://doi.org/10.1016/j.jenvman.2022.115518

[4] M. Shafaee, E.K. Goharshadi, M. Mashreghi, M. Sadeghinia, J. Photochem. Photobiol. A: Chem. 357, 90-102(2018); https://doi.org/10.1016/j.jphotochem.2018.02.019

[5] I. Ahmad, R. Bousbih, A. Mahal, W.Q. Khan, M. Aljohani, M.A. Amin, N.N.A. Jafar, M.S. Jabir, H. Majdi, A.S. Alshomrany, M. Shaban, I. Ali, H. Bayahia, Mater. Sci. Semicond. Process. 180, 108578(2024); https://doi.org/10.1016/j.mssp.2024.108578

[6] M. Liang, A. Shui, Chem. Phys. Impact 8, 100546(2024); https://doi.org/10.1016/j.chphi.2024.100546

[7] H. Yu, M. Zhao, C. Xue, J. Huang, N. Zhao, L. Kong, J. Mol. Struct. 1300, 137272(2024); https://doi.org/10.1016/j.molstruc.2023.137272

[8] C.M. Taylor, A. Ramirez-Canon, J. Wenk, D. Mattia, J. Hazard. Mater. 378, 120799(2019); https://doi.org/10.1016/j.jhazmat.2019.120799

[9] R. Kumar, R.S. Gedam, Ceram. Int. 50, 24716-24724(2024); https://doi.org/10.1016/j.ceramint.2024.04.208

[10] C. Chai, H. Liu, W. Yu, Chem. Phys. Lett. 778, 138765(2021); https://doi.org/10.1016/j.cplett.2021.138765

[11] Y. Rati, Y.N. Hendri, R. Waluyo, F. Zendrato, A.S. Rini, R. Marlina, R. Kurniawan, Y. Darma, Opt. Mater. 135, 113370(2023); https://doi.org/10.1016/j.optmat.2022.113370

[12] M.K. Hussain, N.R. Khalid, M. Tanveer, A. Abbas, F. Ali, W. Hassan, M. Rianna, S. Rahman, M. Hamza, M. Aslam, Opt. Mater. 148, 114794(2024); https://doi.org/10.1016/j.optmat.2023.114794

[13] F. Andish-Lifshagerd, A. Habibi-Yangjeh, M. Habibi, Y. Akinay, J. Photochem. Photobiol. A: Chem. 448, 115351(2024); https://doi.org/10.1016/j.jphotochem.2023.115351

[14] K. He, International J. Hydrogen Energy, 51, 30-40(2024); https://doi.org/10.1016/j.ijhydene.2023.08.050

[15] R. Han, X. Zhang, Z. Shang, S. Chen, Q. Lu, E. Guo, X. Han, G. Zhang, Z. Li, J. Colloid Interface Sci. 662, 822-835(2024); https://doi.org/10.1016/j.jcis.2024.02.132

[16] M. Shekofteh-Gohari, A. Habibi-Yangjeh, J. Ind. Eng. Chem. 44, 174-184(2016); https://doi.org/10.1016/j.jiec.2016.08.028

[17] X. Bai, Z. Fu, X. Ma, Z. Zhang, J. Fan, E. Liu, J. Li, J. Clean. Prod. 369, 133099(2022); https://doi.org/10.1016/j.jclepro.2022.133099

[18] W. Zhang, D. Zhang, Y. Zhang, Journal of Materials Science: Mater. Electron. 31, 6706-6715(2020); https://doi.org/10.1007/s10854-020-03227-8

[19] R. Sharma, S. Sambyal, P. Mandyal, R.S. Islam, A. Priye, I. Kainthla, M. Kumar, V. Chauhan, P. Shandilya, J. Environ. Chem. Eng. 12, 112(2024); https://doi.org/10.1016/j.jece.2024.112126

[20] R. Sharma, S. Sambyal, P. Mandyal, R.S. Islam, A. Priye, I. Kainthla, M. Kumar, V. Chauhan, P. Shandilya, J. Environ. Chem. Eng. 12, 112203(2024); https://doi.org/10.1016/j.jece.2024.112203

[21] Q. Niu, Q. Chen, G. Huang, L. Li, Y. He, J. Bi, J. Colloid Interface Sci. 643, 102-114(2023); https://doi.org/10.1016/j.jcis.2023.04.013

[22] D. Cao, S. Gong, X. Shu, D. Zhu, S. Liang, Nanoscale Res. Lett. 14, 210(2019); https://doi.org/10.1186/s11671-019-3038-3

[23] X. Bai, Z. Fu, X. Ma, Z. Zhang, J. Fan, E. Liu, J. Li, J. Clean. Prod. 369, 133099(2022); https://doi.org/10.1016/j.jclepro.2022.133099

[24] S. Agarwal, L.K. Jangir, K.S. Rathore, M. Kumar, K. Awasthi, Appl. Phys. A, 125, 553(2019); https://doi.org/10.1007/s00339-019-2852-x

[25] T. Thiyagarajan, V. Deivasigamani, M. Raj, C. Joseph, T. Dheivasigamani, B. Palanivel, M.S. Hamdy, M. Shkir, Korean J. Chem. Eng. 38(5), 952-965(2021).
https://doi.org/10.1007/s11814-021-0756-x
[26] C. Chen, W. Bi, Z. Xia, W. Yuan, L. Li, ACS Omega 5, 13185-13195(2020);
https://doi.org/10.1021/acsomega.0c01220